

Toxicity of Mitoxantrone-loaded Superparamagnetic Iron Oxide Nanoparticles in a HT-29 Tumour Spheroid Model

ANNKATHRIN HORNUNG^{1,2}, MARINA POETTNER¹, RALF P. FRIEDRICH¹, BIANCA WEIGEL¹,
STEPHAN DUERR^{1,3}, JAN ZALOGA¹, IWONA CICHA¹, CHRISTOPH ALEXIOU¹ and CHRISTINA JANKO¹

¹Department of Otorhinolaryngology, Head and Neck Surgery,
Section of Experimental Oncology and Nanomedicine (SEON), Else Kröner-Fresenius-Stiftung Professorship,
University Hospital Erlangen, Erlangen, Germany;

²Friedrich-Alexander-University Erlangen-Nuremberg (FAU), Erlangen, Germany;

³Department of Otorhinolaryngology, Section of Phoniatics & Pediatric Audiology,
Head & Neck Surgery, University Hospital Erlangen, Erlangen, Germany

Abstract. *Background/Aim:* Cancer research is commonly carried out in two-dimensional (2D) cell cultures, which poorly reflect in vivo settings where the growing tumours are exposed to mechanical forces and biochemical gradients. In this study we established a HT-29 colon carcinoma tumor spheroid model to investigate the effect of free mitoxantrone (MTO) and its nanoparticle-bound form (SPION^{MTO}) under 3D cell culture conditions. *Materials and Methods:* Tumour spheroids were generated by seeding HT-29 colon carcinoma cells on agarose-coated cell culture wells. Growth of the spheroids was monitored daily by transmission microscopy upon treatment with free MTO, SPION^{MTO} or unloaded SPION. *Results and Conclusion:* Unloaded SPION did not affect the spheroid size compared to untreated controls, while both free MTO and SPION^{MTO} inhibited growth of the spheroids in a dose- and time-dependent manner. In comparison to free MTO, the effect of SPION^{MTO} on spheroid growth was slightly delayed. Further analyses are necessary to investigate if MTO infiltrates spheroids in its

nanoparticle-bound form or whether it is released from SPION before infiltration.

Chemotherapy, surgery and radiotherapy are currently the three pillars that cancer treatment is based on. Conventional chemotherapy is applied (generally intravenously or orally); therefore, only a fraction of the chemotherapeutic agent reaches the tumour region, implying that very high concentrations have to be applied to achieve the necessary therapeutic dose in the tumour. Because conventional cytotoxic drugs were designed for use at maximum tolerated dose in the patients (1, 2), cancer patients are confronted with enormous side-effects as infertility, nausea, anaemia and hair loss, resulting in tremendously reduced quality of life (3). Site-directed chemotherapy using magnetic drug targeting (MDT) might overcome the problem of unspecific distribution of the cytotoxic drug. In MDT, magnetic “nanotransporters” carry their therapeutic cargo precisely to the desired region with the help of an external magnetic field. Generally, the local application and targeted transport of chemotherapeutics using micro- and nanocarrier systems is a promising approach in medicine (4, 5). With this method, therapeutic success has previously been demonstrated in tumour-bearing rabbits (6, 7).

Aiming at localized cancer treatment, our group produces superparamagnetic iron oxide nanoparticles (SPION), which are coated with a layer of lauric acid (LA), and additionally with bovine serum albumin (BSA), to increase stability and biocompatibility. These particles are then loaded with a chemotherapeutic drug (e.g. mitoxantrone (MTO)) and injected intra-arterially in the tumour-supplying vascular system. By inducing a magnetic field, the particles, together with their cytotoxic cargo, are guided to the tumour region and accumulated there (6-9). Due to enhanced permeability of tumour-supplying vessels, the nanoparticles can penetrate and diffuse into the tumour region. In addition to that, a dysfunctional

This article is freely accessible online.

Abbreviations: BSA, bovine serum albumin; FCS, fetal calf serum; SPION, superparamagnetic iron oxide nanoparticle; MDT, magnetic drug targeting; MTO, mitoxantrone.

Correspondence to: Christina Janko, Department of Otorhinolaryngology, Head and Neck Surgery, Section of Experimental Oncology and Nanomedicine (SEON), Else Kröner-Fresenius-Stiftung Professorship, University Hospital Erlangen, Glückstraße 10a, 91054 Erlangen, Germany. Tel: +49 91318533142, Fax: +49 8534808, e-mail: christina.janko@uk-erlangen.de

Key Words: Tumour spheroids, magnetic drug targeting, nanotoxicology, mitoxantrone.

lymphatic drainage in the tumour fosters the formation of a chemotherapeutic/nanoparticle depot that is beneficial for targeted tumour therapy (so called “enhanced permeability and retention” (EPR) effect) (10, 11). Due to the specific enrichment of the chemotherapeutic agent, healthy cells and organs are preserved from the cytotoxic effects (12). For the future translation of these promising animal experiments into clinics, it is necessary to obtain a good understanding of the cellular uptake of these particles, their efficacy and the release mechanisms of drugs coupled to them. Although the performance of SPION has been extensively studied in monolayer cell cultures, the predictive value of 2D *in vitro* experiments is limited and more relevant 3D *in vitro* models are urgently needed (13). To analyze the penetration and effect of SPION and chemotherapeutics-loaded SPION on 3-dimensional structures, we used multicellular tumour spheroids as an *in vitro* model. Tumour cells growing in spheroids show higher degree of morphological and functional differentiation than monolayer cells (14-16). Due to oxygen/nutrients’ gradients and accumulation of catabolites, tumour cells within spheroids have a heterogeneous morphology, proliferation and differentiation (17, 18). The potential of this model system in cancer research and drug delivery has been stressed previously (19, 20) as multicellular tumour spheroids much closer mimic tumour physiology and drug resistance than planar cell cultures (19, 21).

In this study, we tested a colon carcinoma cell line (HT-29), a breast cancer cell line (MCF-7) and a prostate carcinoma cell line (PC-3) for standardized 3D tumour spheroid generation and analyzed growth kinetics of the tumour spheroids. In a further step, the established 3D tumour model was used to investigate the effects of free MTO, nanoparticle-bound MTO and unloaded nanoparticles to gain more knowledge on their performance in a complex cellular system.

Materials and Methods

Synthesis of superparamagnetic iron oxide nanoparticles (SPION). SPIONs were synthesized at the Section of Experimental Oncology and Nanomedicine (SEON), University Hospital Erlangen, as previously described (22). For their further application in cellular studies, SPIONs were coated with lauric acid (LA) and covered by a protein corona of bovine serum albumin (BSA). The resulting SEON-made nanoparticles are further in text called SEON^{LA-BSA}. These particles were subsequently loaded with the chemotherapeutic drug mitoxantrone (MTO; TEVA Pharma, Ulm, Germany), resulting in SEON^{LA-BSA}*MTO. MTO is a cytostatic drug, which intercalates into the DNA causing crosslinks and strand breaks and inhibits the topoisomerase II (11, 23). The comprehensive physicochemical characterization of SEON^{LA-BSA} and SEON^{LA-BSA}*MTO was previously described in Zaloga *et al.* (22).

Cells and culture conditions. Breast cancer MCF-7 cell line, prostate cancer PC-3 cell line and colon carcinoma HT-29 cell line (all from ATCC/LGC GmbH, Wesel, Germany) were tested for spheroid generation. MCF-7 cells were maintained in DMEM without phenol

red supplemented with 10 % foetal calf serum (FCS) and 1% L- Glutamine (all from Biochrom, Berlin, Germany). PC-3 cells were cultured in Ham’s F-12K medium (Gibco®, Life Technologies GmbH, Darmstadt, Germany) supplemented with 10% FCS. HT-29 cells were cultured in McCoy’s 5A medium (Gibco®) supplemented with 10% FCS. All cells were cultivated under standard cell culture conditions in a humidified incubator (INCOmed, Schwabach, Memmert, Germany) at 37°C and 5 % CO₂. For the experiments, the cells were grown to a confluence of 80-90% (approximately 15×10⁶ cells in T75 cm² flasks) and passaged twice a week using 0.25% trypsin/0.02% EDTA in PBS (PAN Biotech, Aidenbach, Germany).

Generation of spheroids. For the spheroid generation, each well of a 96-well plate (Sarstedt, Nümbrecht, Germany) was coated with 30 µl 1.5% agarose gel (Roth, Karlsruhe, Germany). The cells were detached with 2 ml 0.25% trypsin/0.02% EDTA in PBS from the cell culture flasks and then re-suspended in 10 ml medium to form single-cell suspensions. In the next step, the cells were counted and the viability was determined using MUSE® Cell Analyzer (Merck-Millipore, Billerica, MA, USA). In order to create spheroids of different sizes, the cell suspensions were diluted with medium to obtain the respective cell numbers. Then, 100 µl medium and 100 µl cell suspension were added to each agarose-coated well. For optimal cell distribution, the plates were rotated several times. Then, the cells were cultivated for up to 14 days in a humidified incubator at 37°C and 5% CO₂.

Analysis of spheroid growth kinetics via microscopy. Growth of the spheroids was investigated using an Axiovert 40 CFL Microscope (Zeiss, Jena, Germany) with a 2.5× objective. All 24-h pictures of the spheroids were taken with the Axio Vision SE64 Rel4.9 software (Zeiss). The size of the spheroids was assessed using the Image J Software (National Institutes of Health, Bethesda, MD, USA) and an objective calibration slide in order to calculate the spheroid area. Data analysis was performed in MS Excel.

Treatment with MTO, SEON^{LA-BSA} and SEON^{LA-BSA}*MTO. Three different dilutions of MTO, SEON^{LA-BSA}*MTO and SEON^{LA-BSA} (in corresponding iron concentrations) were pipetted to the HT-29 spheroids 72 h after spheroid generation, resulting in the indicated concentrations (Figure 4a). All spheroids were incubated for an additional 4-day period under standard cell culture conditions. Transmission microscopy pictures were taken every 24 h and analysed by the Image J software.

Results

As the 3D spheroid model is more suitable for monitoring the effects of chemotherapy *in vitro* than planar cell cultures, the aim of this pilot study was to establish a 3D tumour model with reproducible spheroid sizes and to perform first nanotoxicological tests with MTO, SEON^{LA-BSA}*MTO and SEON^{LA-BSA}.

To establish a stable and reproducible 3D tumour model, we tested the three cancer cell lines MCF-7, PC-3 and HT-29 for their ability to form multicellular spheroids. For spheroid formation, agarose-coated wells were used to prevent cells from attaching to the bottom of the cell culture well and to

increase interactions with neighbouring cells. Manual rotation of the 96-well plate guaranteed that all cells in the well accumulated in the centre for spheroid formation (Figure 1).

Daily monitoring of spheroid formation and growth using phase-contrast microscopy showed that PC-3, MCF-7 and HT-29 cells formed completely different spheroid structures, as depicted in Figure 2.

PC-3 cells formed loose cell aggregates, which could easily be dissolved by mechanical force. These spheroids were flat broad discs and their shape did not change within 10 days of observation. The spheroids proliferated very uniformly in a cell number- and time-dependent manner. With time, growth kinetics data became quite imprecise as PC-3 aggregates became too large for observation by microscopy with a $2.5\times$ objective. Therefore, after 7 days, we abandoned the analysis of growth by transmission microscopy (Figure 2a).

MCF-7 cells, in contrast, had already formed quite compact globular structures 24 h after seeding. However, the shape of the spheroids was rather inhomogeneous and all spheroids differed morphologically from one another (Figure 2b). Transmission microscopy and calculation of the spheroid area revealed a cell count- and time-dependent increase in spheroid size with relatively high standard deviations, especially at higher cell numbers. Due to this inhomogeneity, MCF-7 cells were not optimal for further assays with anticancer drugs or nanoparticles.

Another cell line we tested for spheroid formation was the colon carcinoma cell line HT-29. Initially, HT-29 cells formed loose cell aggregates but, over time, these cells produced a compact cell assembly, as shown by the reduction of spheroid area (Figure 2c). After 72 h, compact round spheroids had already formed. The morphology of the HT-29 tumour spheroids appeared consistent and growth of the spheroids continued steadily during the experiment (Figure 2c). After ten days of observation, spheroids of different sizes had formed dependent on the number of seeded cells. The sizes of the spheroids with similar amounts of seeded cells were very homogenous, as reflected by minimal standard deviations. Moreover, the spheroids were also resistant to gentle movement and transportation of the plates, which facilitated their handling. Consequently, HT-29 spheroids were chosen for further use in nanotoxicological testing.

Selection of culture conditions for HT-29 spheroids. The generation of multicellular tumour spheroids with homogenous sizes is essential for further toxicological screening procedures. Although monolayer cultures of HT-29 cells had been performed extensively in our lab, optimal conditions for HT-29 spheroid cultures had to be evaluated. For that purpose, different cell numbers were seeded to generate spheroids of various volumes as shown in Figure 3. Observation started 72 h after seeding to ensure that the cells

had already formed tight and compact spheroids. The experiments revealed that HT-29 spheroids continuously grew for about 10 days until they reached the plateau phase. At this time point, the spheroids of different cell numbers converged in size as the initially smaller spheroids showed a prolonged growth phase, whereas the initially bigger spheroids slowed down their growth phase earlier. The spheroids with the highest seeded cell number already started to degrade at the end of the observation period. The final sizes of the spheroids ranged between $0.35\text{-}0.42\text{ mm}^2$ (Figure 3a). To determine whether decrease of growth depends on lack of nutrition due to consumption of medium ingredients and an increase of cell metabolism products, we changed the cell culture medium of half of the spheroid preparations after 10 days (Figure 3b). The monitoring was further continued for 4 days, showing that spheroid growth was comparable to the untreated control spheroids (Figure 3a), indicating only minor differences between growth kinetics in the two different settings. Overall, corresponding cell numbers showed similar curve progressions (for 2,000 to 10,000 cells seeded) and, in both set-ups, the same size range for all spheroids was finally obtained (Figure 3a and b). Only the behaviour of spheroids formed by 12,000 cells was altered by the medium exchange: After 10 days, these spheroids maintained their size and did not show any signs of degradation after incubation for an additional 4-day period. Since medium exchange did not influence spheroid morphology for samples with smaller cell numbers, we decided to omit this step to prevent potential disruption of the spheroids by pipetting. For all further experiments, 6,000 cells were selected as starting condition, since a consistent growth was detected until day 10.

To analyze inter-assay comparability, three independent experiments with at least $n\geq 15$ spheroids (with starting number of 6,000 cells each) were performed in the further studies. Due to the consistent globular structure of the HT-29 spheroids, calculation of spheroid diameters in μm was possible based on the data for spheroid areas in mm^2 . With time, HT-29 spheroids, within all three experiments, consistently grew and displayed a high homogeneity in size as reflected by small standard deviations and Spearman's R^2 values (Table I). Thus, these experiments were quite reproducible and comparable with each other as shown in Figure 3c, constituting a perfect starting system for nanotoxicity screening experiments.

*Cytotoxic effect of MTO, SEON^{LA-BSA} and SEON^{LA-BSA}*MTO on HT-29 spheroids.* The effect of pure MTO, SEON^{LA-BSA}*MTO and nanoparticles without MTO (SEON^{LA-BSA}) was examined using HT-29 spheroids. At 72 h after seeding, as HT-29 cells had formed tight spheroids, three different final concentrations of free MTO and nanoparticle-bound MTO (0.05 $\mu\text{g/ml}$, 0.5 $\mu\text{g/ml}$, 5 $\mu\text{g/ml}$) were added to the

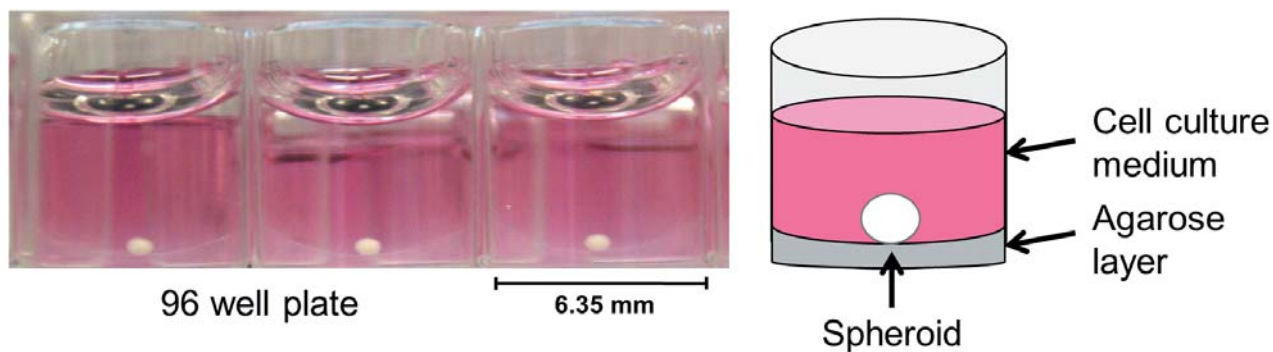


Figure 1. Spheroid formation using agarose coating. Wells of a 96-well plate were coated with 30 μ l agarose forming a non-adherent concave layer, thus preventing cell attachment to the surface and inducing spheroid formation. Shown are HT-29 spheroids that have been grown for 14 days. Left: Macroscopic picture, spheroid is visible to the unaided eye. Right: Scheme of set-up for spheroid formation.

Table I. Reproducibility and inter-assay comparability of spheroid growth.

HT-29 spheroid area in mm²

	Mean \pm standard deviation					y	R ²
	72 h	96 h	120 h	144 h	168 h		
Exp. 1 (n=16)	0.235 \pm 0.010	0.258 \pm 0.009	0.288 \pm 0.011	0.338 \pm 0.011	0.369 \pm 0.015	0.0014x+0.1236	0.9829
Exp. 2 (n=15)	0.209 \pm 0.056	0.242 \pm 0.065	0.276 \pm 0.074	0.307 \pm 0.082	0.337 \pm 0.090	0.0013x+0.1145	0.9995
Exp. 3 (n=16)	0.213 \pm 0.016	0.250 \pm 0.012	0.279 \pm 0.014	0.232 \pm 0.015	0.345 \pm 0.016	0.0014x+0.1133	0.9924

HT-29 spheroid diameter in μ m

	Mean \pm standard deviation					y	R ²
	72 h	96 h	120 h	144 h	168 h		
Exp. 1 (n=16)	547 \pm 12	573 \pm 10	605 \pm 12	656 \pm 10	685 \pm 14	1.4986x+433.48	0.9872
Exp. 2 (n=15)	532 \pm 21	573 \pm 23	611 \pm 23	644 \pm 21	675 \pm 27	1.4911x+428.18	0.9967
Exp. 3 (n=16)	520 \pm 20	564 \pm 14	596 \pm 15	641 \pm 15	662 \pm 15	1.5081x+415.77	0.9894

cell culture media. As controls, the unloaded nanoparticles were applied at the concentrations corresponding to iron concentrations of MTO-loaded nanoparticles (Figure 4a). Spheroid size was normalized to 100% at the beginning of the treatment and the effect of treatment on spheroid growth was given in % (Figure 4b). As expected, untreated spheroids had consistent growth behaviour within the observation period of 4 days. The calculated growth curves (Figure 4b) revealed that both free MTO and SEON^{LA-BSA}*MTO resulted in a dose-dependent size reduction of the treated spheroids, as compared to the untreated controls.

A significant effect was observed at the lowest concentration of MTO whereby the spheroids treated with 0.05 μ g/ml of MTO or SEON^{LA-BSA}*MTO displayed a decreased growth after 48 hours of treatment, while spheroid

treatment with higher MTO concentrations (0.5 and 5.0 μ g/ml) induced a complete inhibition of growth from the beginning of treatment. Here, an increase in spheroid size was recorded 48 h after the treatment again, which might be due to the fact that cell-cell contacts dissolved and dead cells were released from the cell association causing a loose spheroid appearance. The erosion of the spheroids upon MTO-treatment could be clearly observed in the transmission microscopic pictures (Figure 4c). The unloaded SEON^{LA-BSA} nanoparticles in the corresponding iron concentrations did not influence the spheroid size and morphology. Thus, it became evident that the cytotoxic effect of SEON^{LA-BSA}*MTO was caused by the chemotherapeutic cargo and not by the nanoparticles themselves. As compared to free MTO, nanoparticle-bound MTO (SEON^{LA-BSA}*MTO) had a slightly delayed effect on

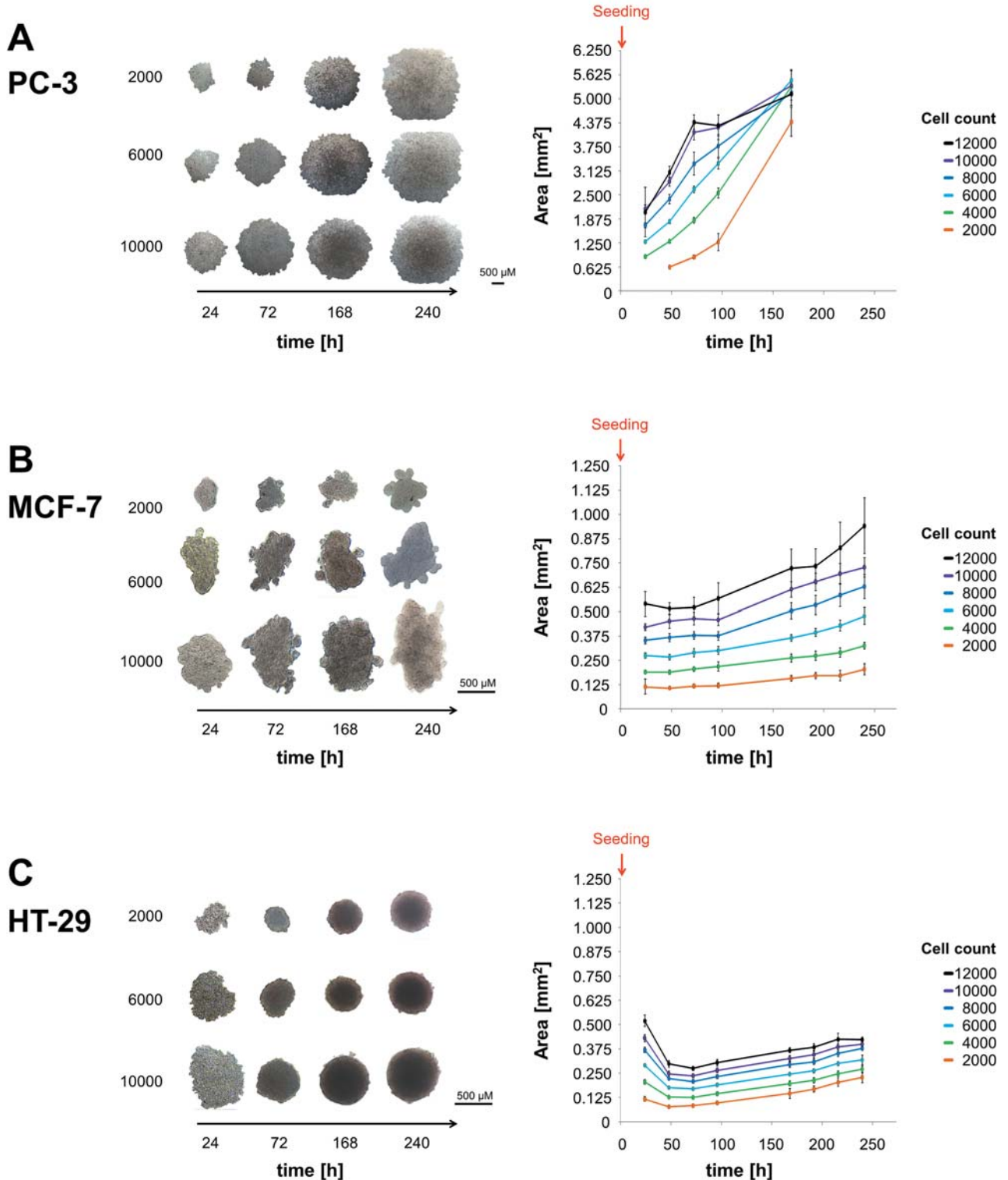


Figure 2. Morphology and growth kinetics of spheroids formed by the PC-3, MCF-7 and HT-29 cell lines. Various cell numbers (2,000, 4,000, 6,000, 8,000, 10,000, 12,000) of each cell line were seeded into agarose-coated 96-well plates. Spheroid growth was documented by transmission microscopic pictures followed by calculation of the spheroid area using Image J software. Left: Representative pictures for 2,000, 6,000, 10,000 cells are shown. Right: Kinetics of spheroid growth as shown by spheroid area estimation (mm²). Depicted are the mean values of $n \geq 10$ spheroids with standard deviations. Note: Due to the excessively large area of PC-3 aggregates, the scale bars are different from the HT-29 and MCF-7 scale bars.

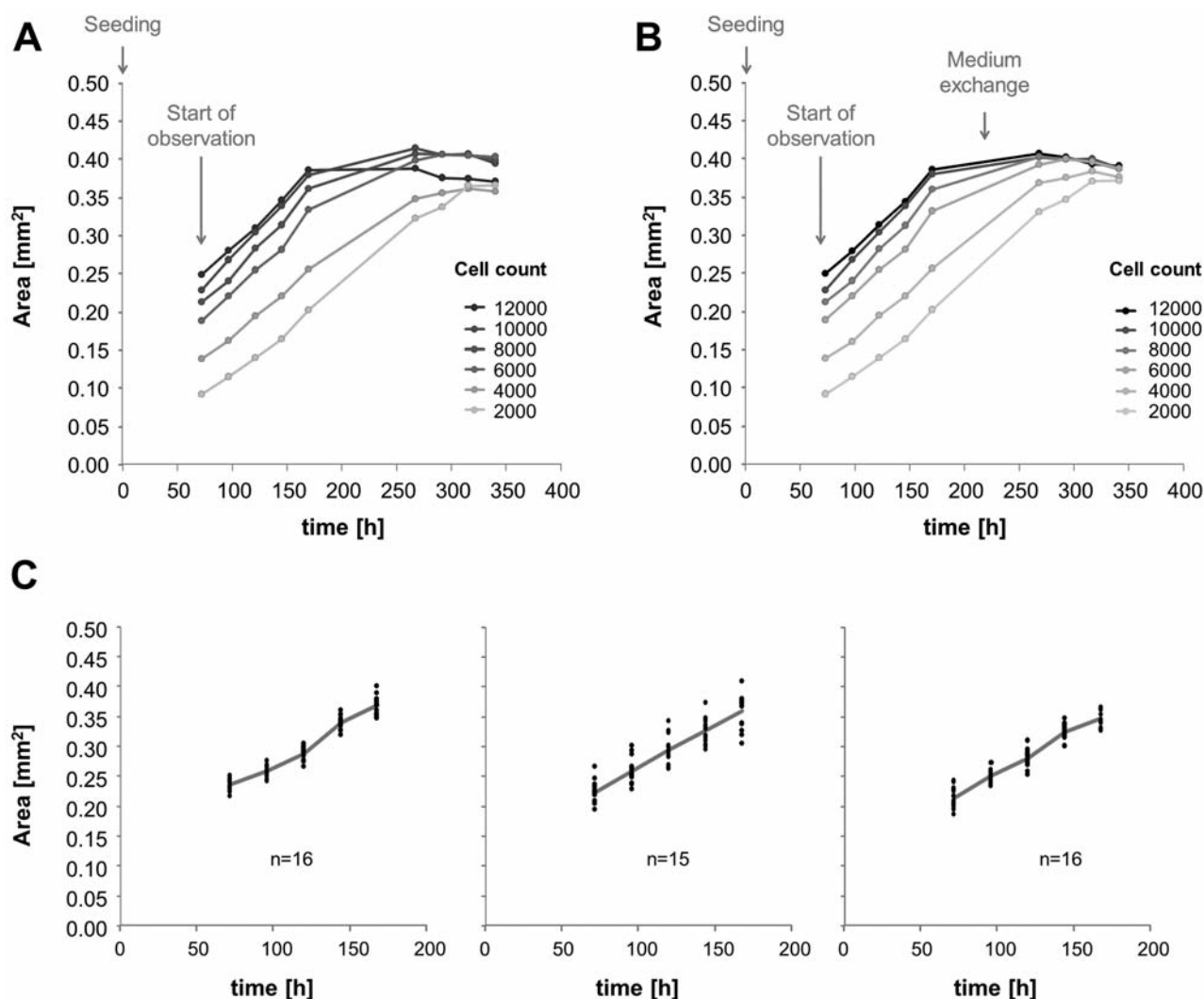


Figure 3. Proliferation of HT-29 spheroids and selection of suitable cell culture conditions. HT-29 cells were seeded into agarose-coated 96-well plates and cultivated for 14 days. Starting on day 3, transmission microscopy was performed to monitor spheroid proliferation; spheroid area was calculated by Image J software. After 10 days, no medium exchange (A) or a medium exchange (B) was performed. Shown are the mean values of $n \geq 8$ spheroids each. (C) Comparison of spheroid sizes of $n \geq 15$ spheroids of three independent experiments (days 3-7). Every black dot represents a spheroid, while red lines show the mean values of spheroid sizes at the respective time points.

spheroid growth inhibition, possibly indicating that free MTO could penetrate faster into the spheroid.

Discussion

To analyze drug penetration into a 3D tumour structure, tight packaging of cells, as well as reproducible spheroid diameters, are prerequisites (24). In this study, we generated multicellular tumour spheroids of HT-29 cells of reproducible size and morphology, whereas the spheroids formed by MCF-7 and PC-3 were not suitable for further experimental procedures because of their morphological

heterogeneity and inadequate compactness, respectively. As also described by others, the spontaneous formation of tight spheroids is restricted to few cell lines, whereas many tumour cell types grow only as aggregates with weak cell-cell contacts when cultured in a 3D setting (25, 26). This problem might be overcome by the addition of reconstituted basement membrane, which was reported to induce spherical spheroid formation in PC-3 and MCF-7 cells as well (25). Various culture techniques have been described to generate spheroids (27, 28) and shown that spheroid size and growth strongly depend on the number of seeded cells (29). Our present data confirmed that modulation of

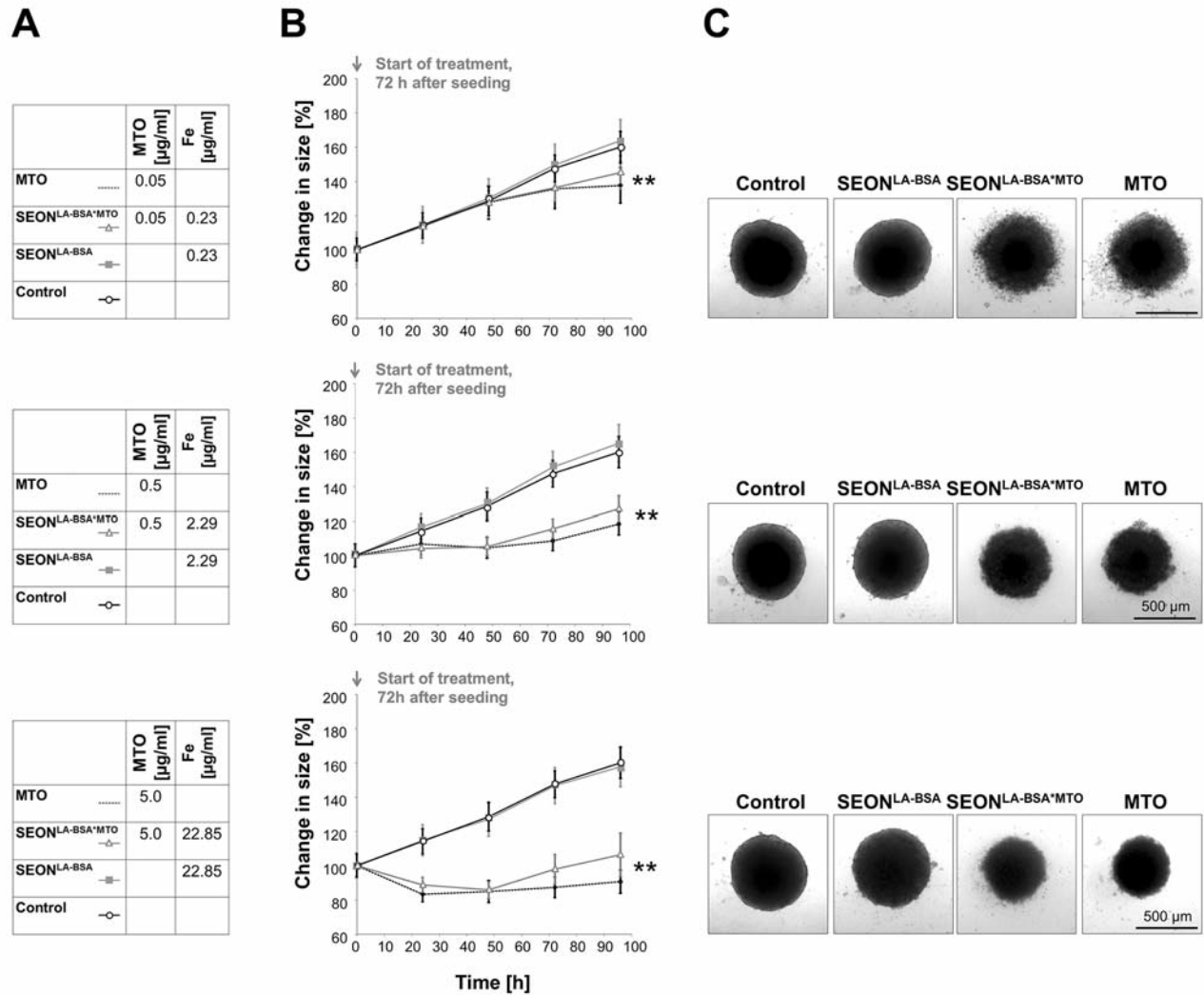


Figure 4. Cytotoxic effect of MTO, SEON^{LA-BSA}*MTO and SEON^{LA-BSA} on HT-29 spheroids. Spheroids were grown with 6,000 HT-29 cells per well for 72 h and, subsequently, treated with MTO, SEON^{LA-BSA}*MTO and SEON^{LA-BSA} as indicated (left). Untreated spheroids served as controls. Spheroid growth was documented by transmission microscopy (right) followed by calculation of the spheroid area using Image J software (middle). Shown are the mean values of three independent experiments (with $n=16$ spheroids per condition) and standard deviations ($p \leq 0.001$, Student's *t*-test).

spheroid size can be performed easily and that spheroid formation on agarose-coated wells represents a reproducible method to obtain compact 3D aggregates within 72 h. 3D *in vitro* models have been shown to reflect the *in vivo* response to therapeutic agents more accurately than conventional cell culture systems (30). Especially with regard to the involvement of tumour-specific features as multicellularity-mediated resistance to anticancer agents, 3D models must be used since this property is often absent in a monolayer culture (31, 32). Also, diffusion gradients of drugs from the outside to the inside of the spheroid may determine the experimental outcome (33). Treating

spheroids with pure MTO, SEON^{LA-BSA}*MTO and SEON^{LA-BSA} showed a time and concentration dependent effect of MTO and SEON^{LA-BSA}*MTO, whereas the unloaded SEON^{LA-BSA} nanoparticles were very well tolerated. Similar to former studies with 2D cell cultures, our present experiments confirmed that these unloaded iron oxide nanoparticles had no apparent impact on the cells in therapeutically-relevant doses (22, 34, 35).

The effect of MTO was stronger compared to SEON^{LA-BSA}*MTO, possibly because of delayed drug penetration in its nanoparticle-bound form. Interestingly, comparing the effect of MTO and SEON^{LA-BSA}*MTO in suspension-grown Jurkat

T-cells, no delayed effect of the nanoparticle-bound MTO was shown. On the contrary, the combination of nanoparticles and MTO showed a synergistic effect on cell death induction (22). It has been speculated that the extracellular matrix prevents nanoparticles larger than 100 nm in diameter from penetration into tumour spheroids. In line with these suggestions, the coating of nanoparticles with collagenase, an enzyme that breaks the peptide bonds of extracellular matrix, was shown to improve nanoparticle delivery (36). Since our nanoparticles, either unloaded or loaded with MTO, are below 100 nm in size, this should not be a chief limiting factor for the spheroid penetration.

Experimental evidence has proven that mass transport within multicellular tumour spheroids is similar to avascular tissue or tumour mass, with diffusion limitation of about 150-200 μm to many molecules (O_2 , nutrients, metabolic waste) (37). Therefore, a spheroid bigger than 500 μm in diameter usually has a necrotic core surrounded by a viable rim, which consists of an inner layer of quiescent cells and an outer layer of proliferating cells (27). In our study, the spheroids were treated 72 h after seeding and the untreated spheroids exhibited a constant growth behaviour during the observation period of four further days. At the end of the experimental period, the spheroids had reached an area of approximately 0.35 mm^2 , which corresponds to a diameter of 670 μm . Due to the large size of our spheroids, we speculate that their mass transport can be limited and that the microenvironment inside of the spheroids could induce necrosis. In future studies, it will be necessary to analyse the spheroid phenotype *e.g.* by analysis of single cell suspensions using flow cytometry or by staining of spheroid sections for fluorescence microscopy (38). Taken together, we conclude that multicellular tumour spheroids constitute an important advancement over 2D tumour cell cultures for drug delivery and toxicity testing of drug-loaded nanoparticles. Moreover, the 3D tumour models provide experimental settings that are much closer to the *in vivo* situation where tumour cells form close cell-cell contacts and are exposed to different types of mechanical forces and biochemical gradients.

Disclosure

The Authors report no conflicts of interest in this work.

Acknowledgements

This study was supported by the Bavarian State Ministry of the Environment and Consumer Protection and by the Deutsche Forschungsgemeinschaft (DFG) through the Cluster of Excellence Engineering of Advanced Materials. The present work was performed in fulfilment of the requirements for obtaining the degree "Dr. med."

References

- Baruchel S and Stempak D: Low-dose metronomic chemotherapy: myth or truth? *Onkologie* 29: 305-307, 2006.
- Shimizu K and Oku N: Cancer anti-angiogenic therapy. *Biol Pharm Bull* 27: 599-605, 2004.
- Giesinger JM, Wintner LM, Zabernigg A, Gamper EM, Oberguggenberger AS, Sztankay MJ, Kemmler G and Holzner B: Assessing quality of life on the day of chemotherapy administration underestimates patients' true symptom burden. *BMC cancer* 14: 758, 2014.
- Owen J, Pankhurst Q and Stride E: Magnetic targeting and ultrasound mediated drug delivery: benefits, limitations and combination. *Int J Hyperthermia* 28: 362-373, 2012.
- Polyak B and Friedman G: Magnetic targeting for site-specific drug delivery: applications and clinical potential. *Expert Opin Drug Deliv* 6: 53-70, 2009.
- Lyer S, Tietze R, Jurgons R, Struffert T, Engelhorn T, Schreiber E, Dörfler A and Alexiou C: Visualisation of tumour regression after local chemotherapy with magnetic nanoparticles - a pilot study. *Anticancer Res* 30: 1553-1557, 2010.
- Tietze R, Lyer S, Durr S, Struffert T, Engelhorn T, Schwarz M, Eckert E, Goen T, Vasylyev S, Peukert W, Wiekhorst F, Trahms L, Dorfner A and Alexiou C: Efficient drug-delivery using magnetic nanoparticles-biodistribution and therapeutic effects in tumour bearing rabbits. *Nanomedicine* 9: 961-971, 2013.
- Alexiou C, Tietze R, Schreiber E, Jurgons R, Richter H, Trahms L, Rahn H, Odenbach S and Lyer S: Cancer Therapy with Drug Loaded Magnetic Nanoparticles- Magnetic Drug Targeting. *J Magn Magn Mater* 323: 1404-1407, 2011.
- Tietze R, Jurgons R, Lyer S, Schreiber E, Wiekhorst F, Eberbeck D, Richter H, Steinhoff U, Trahms L and Alexiou C: Quantification of drug-loaded magnetic nanoparticles in rabbit liver and tumor after *in vivo* administration. *J Magn Magn Mater* 321: 1465-1468, 2009.
- Danhier F, Feron O and Preat V: To exploit the tumor microenvironment: Passive and active tumor targeting of nanocarriers for anti-cancer drug delivery. *J Control Release* 148: 135-146, 2010.
- Frank P and Novak RF: Mitoxantrone and bisantrene inhibition of platelet aggregation and prostaglandin E2 production *in vitro*. *Biochem Pharmacol* 34: 3609-3614, 1985.
- Janko C, Durr S, Munoz LE, Lyer S, Chaurio R, Tietze R, Lohneisen Sv, Schorn C, Herrmann M and Alexiou C: Magnetic drug targeting reduces the chemotherapeutic burden on circulating leukocytes. *Int J Mol Sci* 14: 7341-7355, 2013.
- Abbott A: Cell culture: biology's new dimension. *Nature* 424: 870-872, 2003.
- Gomez-Lechon MJ, Jover R, Donato T, Ponsoda X, Rodriguez C, Stenzel KG, Klocke R, Paul D, Guillen I, Bort R and Castell JV: Long-term expression of differentiated functions in hepatocytes cultured in three-dimensional collagen matrix. *J Cell Physiol* 177: 553-562, 1998.
- Griffith LG and Swartz MA: Capturing complex 3D tissue physiology *in vitro*. *Nat Rev Mol Cell Biol* 7: 211-224, 2006.
- Mayer B, Klement G, Kaneko M, Man S, Jothy S, Rak J and Kerbel RS: Multicellular gastric cancer spheroids recapitulate growth pattern and differentiation phenotype of human gastric carcinomas. *Gastroenterology* 121: 839-852, 2001.

- 17 Carlsson J and Acker H: Relations between pH, oxygen partial pressure and growth in cultured cell spheroids. *International journal of cancer. Int J Cancer* 42: 715-720, 1988.
- 18 Thoma CR, Zimmermann M, Agarkova I, Kelm JM and Krek W: 3D cell culture systems modeling tumor growth determinants in cancer target discovery. *Adv Drug Deliv Rev* 69-70: 29-41, 2014.
- 19 Hirschhaeuser F, Menne H, Dittfeld C, West J, Mueller-Klieser W and Kunz-Schughart LA: Multicellular tumor spheroids: an underestimated tool is catching up again. *J Biotechnol* 148: 3-15, 2010.
- 20 Mehta G, Hsiao AY, Ingram M, Luker GD and Takayama S: Opportunities and challenges for use of tumor spheroids as models to test drug delivery and efficacy. *J Control Release* 164: 192-204, 2012.
- 21 Wenzel C, Riefke B, Grundemann S, Krebs A, Christian S, Prinz F, Osterland M, Golfier S, Rase S, Ansari N, Esner M, Bickle M, Pampaloni F, Mattheyer C, Stelzer EH, Parczyk K, Prechtel S and Steigemann P: 3D high-content screening for the identification of compounds that target cells in dormant tumor spheroid regions. *Exp Cell Res* 323: 131-143, 2014.
- 22 Zaloga J, Janko C, Nowak J, Matuszak J, Knaup S, Eberbeck D, Tietze R, Unterweger H, Friedrich RP, Duerr S, Heimke-Brinck R, Baum E, Cicha I, Dörje F, Odenbach S, Lyer S, Lee G and Alexiou C: Development of a lauric acid/albumin hybrid iron oxide nanoparticle system with improved biocompatibility. *Int J Nanomedicine* 9: 4847-4866, 2014.
- 23 Kapuscinski J, Darzynkiewicz Z, Traganos F and Melamed MR: Interactions of a new antitumor agent, 1,4-dihydroxy-5,8-bis[[2-[(2-hydroxyethyl)amino]-ethyl]amino]-9,10-anthracenedione e, with nucleic acids. *Biochem Pharmacol* 30: 231-240, 1981.
- 24 Grantab R, Sivananthan S and Tannock IF: The penetration of anticancer drugs through tumor tissue as a function of cellular adhesion and packing density of tumor cells. *Cancer Res* 66: 1033-1039, 2006.
- 25 Ivascu A and Kubbies M: Rapid generation of single-tumor spheroids for high-throughput cell function and toxicity analysis. *J Biomol Screen* 11: 922-932, 2006.
- 26 Ivascu A and Kubbies M: Diversity of cell-mediated adhesions in breast cancer spheroids. *Int J Oncol* 31: 1403-1413, 2007.
- 27 Lin RZ and Chang HY: Recent advances in three-dimensional multicellular spheroid culture for biomedical research. *Biotechnol J* 3: 1172-1184, 2008.
- 28 Santini MT and Rainaldi G: Three-dimensional spheroid model in tumor biology. *Pathobiology* 67: 148-157, 1999.
- 29 Charoen KM, Fallica B, Colson YL, Zaman MH and Grinstaff MW: Embedded multicellular spheroids as a biomimetic 3D cancer model for evaluating drug and drug-device combinations. *Biomaterials* 35: 2264-2271, 2014.
- 30 Pampaloni F, Reynaud EG and Stelzer EH: The third dimension bridges the gap between cell culture and live tissue. *Nat Rev Mol Cell Biol* 8: 839-845, 2007.
- 31 Graham CH, Kobayashi H, Stankiewicz KS, Man S, Kapitain SJ and Kerbel RS: Rapid acquisition of multicellular drug resistance after a single exposure of mammary tumor cells to antitumor alkylating agents. *J Natl Cancer Inst* 86: 975-982, 1994.
- 32 Kunz-Schughart LA, Freyer JP, Hofstaedter F and Ebner R: The use of 3-D cultures for high-throughput screening: the multicellular spheroid model. *J Biomol Screen* 9: 273-285, 2004.
- 33 Ward JP and King JR: Mathematical modelling of drug transport in tumour multicell spheroids and monolayer cultures. *Math Biosci* 181: 177-207, 2003.
- 34 Durr S, Lyer S, Mann J, Janko C, Tietze R, Schreiber E, Herrmann M and Alexiou C: Real-time cell analysis of human cancer cell lines after chemotherapy with functionalized magnetic nanoparticles. *Anticancer Res* 32: 1983-1989, 2012.
- 35 Unterweger H, Tietze R, Janko C, Zaloga J, Lyer S, Durr S, Taccardi N, Goudouri OM, Hoppe A, Eberbeck D, Schubert DW, Boccaccini AR and Alexiou C: Development and characterization of magnetic iron oxide nanoparticles with a cisplatin-bearing polymer coating for targeted drug delivery. *Int J Nanomedicine* 9: 3659-3676, 2014.
- 36 Goodman TT, Olive PL and Pun SH: Increased nanoparticle penetration in collagenase-treated multicellular spheroids. *Int J Nanomedicine* 2: 265-274, 2007.
- 37 Curcio E, Salerno S, Barbieri G, De Bartolo L, Drioli E and Bader A: Mass transfer and metabolic reactions in hepatocyte spheroids cultured in rotating wall gas-permeable membrane system. *Biomaterials* 28: 5487-5497, 2007.
- 38 Ma HL, Jiang Q, Han S, Wu Y, Cui Tomshine J, Wang D, Gan Y, Zou G and Liang XJ: Multicellular tumor spheroids as an *in vivo*-like tumor model for three-dimensional imaging of chemotherapeutic and nano material cellular penetration. *Mol Imaging* 11: 487-498, 2012.

Received March 24, 2016

Revised April 22, 2016

Accepted April 25, 2016